Bulletin of the Seismological Society of America, Vol. 92, No. 8, pp. 3080–3086, December 2002

Imaging Crustal Structure along Refraction Profiles Using Multicomponent Recordings of First-Arrival Coda

by Igor B. Morozov*, Scott B. Smithson, and Leonid N. Solodilov

Abstract In a way similar to receiver function imaging, coda of the first arrivals can be used to constrain crustal structure along controlled-source refraction profiles with multicomponent recording. Stacked cross-correlations of the radial and vertical components of recordings from three peaceful nuclear explosions of the 3850-km long profile QUARTZ (Russia) exhibit good correlation with the depth to the basement and provide a horizontal resolution level close to recording station spacing (10–15 km). The results also suggest high (~0.35–0.4) average Poisson's ratios within the sediments. When applied to other multicomponent long-range refraction profiles, this approach could provide a simple and inexpensive way to constrain the structure of the upper crust that is required for interpretation of the deeper structures and that cannot be constrained by other means. Most importantly, reverberations within the sedimentary column appear to account for much of the observed complexity of the first-arrival waveforms, and therefore, such reverberations should be taken into account in the interpretations of seismic scattering from within the mantle.

Introduction

Analysis of the coda of the first teleseismic arrivals using receiver function (RF) methods has become a standard technique for mapping crustal thickness (Langston, 1977; Ammon, 1991). The elegance and power of the receiver function approach is in its ability to use deconvolution of vertical- and horizontal-component recordings of teleseismic arrivals at a single station to neutralize the effect of seismic source. Isolation of source effects results in a RF that is interpreted (albeit with some ambiguity, cf. Ammon *et al.*, [1990]) in terms of a layered crustal velocity structure. In recent years, teleseismic receiver functions of regional seismic arrays were successfully used to image subtle variations of the lithospheric and mantle discontinuities down to the mantle transition zone (e.g., Vinnik, 1977; Bostock, 1996; Dueker and Sheehan, 1998; Chevrot *et al.*, 1999; Gurrola and Minster, 2000). However, with its broad scope of application, RF analysis is still employed exclusively in natural-source, teleseismic seismology, whereas many existing controlled-source, long-range refraction profiles with three-component recording could also benefit in imaging near-receiver structures using this technique. Among such long-range profiles with great potential for RF imaging are the Deep Probe, SAREX (Henstock *et al.*, 1998), and a number of deep seismic sounding (DSS) profiles in Russia (Yegorkin, 1992).

*Department of Geological Sciences, University of Saskatchewan, Saskatoon, SK S7N 5E2, Canada.

Peaceful nuclear explosion (PNE) recordings along ultra-long refraction/reflection profiles in the former Soviet Union (e.g., Ryaboy, 1989) resulted in extensive three-component data sets suitable for short-period coda analysis. Along with regional and teleseismic recordings of PNEs to over 3000-km distance, detailed DSS, industry seismic, and borehole data allow correlation of the results with the structure of the crust (Yegorkin, 1992; A. V. Yegorkin, 1994, personal comm.). As in earthquake studies, recording of several PNEs at each station allows stacking for noise reduction and for further isolation of source and recording site effects. In principle, the controlled-source nature of the experiments offers an advantage over the natural-source RF, allowing examination of the records across linear arrays of hundreds of densely spaced stations from close proximity to teleseismic distances from the source. In this note, we illustrate the use of the coda analysis on one of the most well known profiles of the DSS program, QUARTZ (Fig. 1). For detailed information about this profile and recent interpretations using a broad range of techniques, see Egorkin and Mikhaltsev (1990), Mechie *et al.* (1993), Ryberg *et al.* (1995, 1996), Tittgemeyer *et al.* (1996), Schueller *et al.* (1997), Morozov *et al.* (1998a,b), Morozova *et al.* (1999, 2000), and Morozov and Smithson (2000).

Figure 2 shows the effect of the crustal structure on the first arrivals from PNE QUARTZ-4 between 2800 and 3100 km distances. Compared to the virtually sediment-free Baltic Shield (Kola Peninsula), the thick sedimentary rocks of the

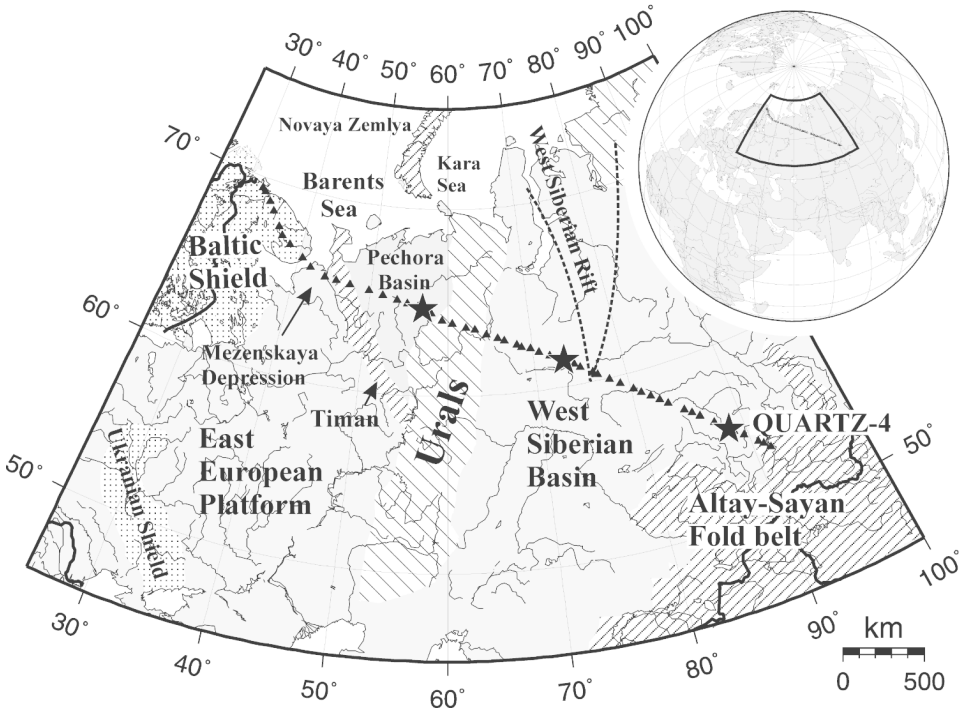

Figure 1. Map of the western part of the former Soviet Union showing the profile QUARTZ. Triangles and stars indicate the locations of the chemical and peaceful nuclear explosions (PNEs) recorded by the profile, respectively. Three QUARTZ PNEs used in this study are labeled, and the major tectonic structures crossed by the profile are indicated. Inset shows the location of the map in Northern Eurasia.

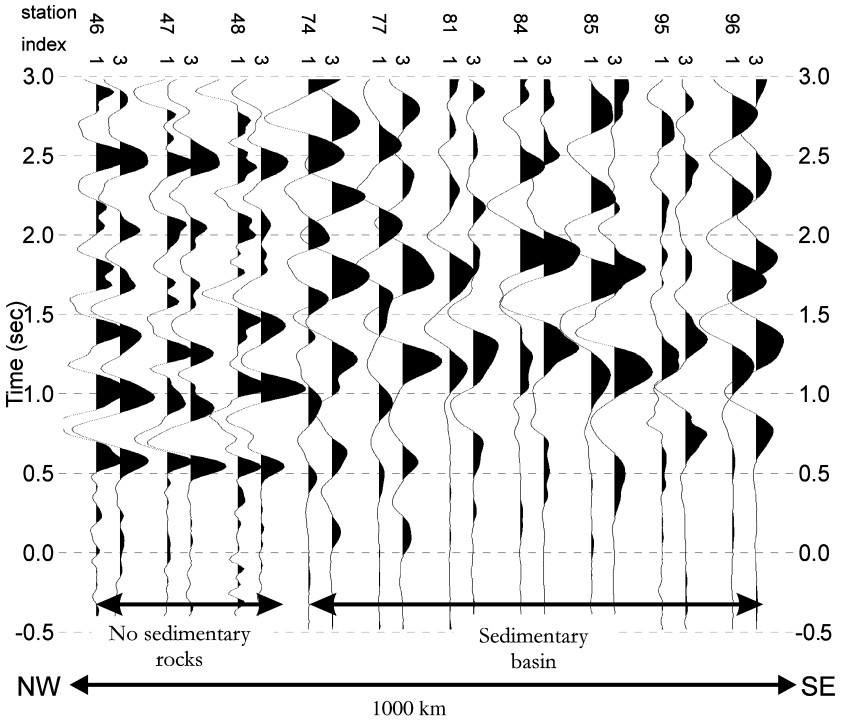

Figure 2. First arrivals from PNE QUARTZ-4 recorded from Kola Peninsula (labeled Baltic Shield in Fig. 1; stations 1–55) to the Mezenskaya depression. Radial-component traces are labeled 1, and vertical-component traces are labeled 3. The PNE source signature is multicyclic (∼2–3 sec long) and emergent in character, with peak energy arriving ∼1–1.5 sec after the onset. Note that the three components of recordings within the first 1–2 sec of the records are generally more coherent within the sediment-free part of the section.

Mezenskaya depression and Pechora basin (Fig. 1), lead to lower-frequency and more complex first arrivals, with the horizontal-component recordings becoming less synchronous with the vertical-component and exhibiting ~0.3- to 0.5-sec delays after the primary onsets (Fig. 2). A likely explanation of such delayed arrivals recorded in horizontal components is their origin in *P/S* mode conversions and/or *P*-wave reverberations within the crust, and particularly within the sedimentary cover. As our following analysis shows, this is indeed the case, and stacked cross correlations of the radial and vertical recordings of the three QUARTZ PNEs result in a consistent image of the basement. Thus, similar to natural-source RF studies, by using the waveforms from a few distant explosions, we are able to obtain a detailed image of the sediment cover along the entire profile.

Another important implication of our results below is in emphasizing the importance of crustal reverberations for interpreting the complexity of long-range seismic arrivals. Recently, a number of authors (Ryberg *et al.*, 1995, 2000; Thybo and Perchuc, 1997) interpreted waveform complexity and the early coda (<10–20 sec) of the arrivals from long-range, controlled-source profiles as indicators of seismic scattering originating within the mantle. In contrast to this hypothesis, our results suggest that at least the first 5–10 sec of the codas of first arrivals carry a pronounced signature of the primary *P*-wave reverberations within the sedimentary column. Furthermore, Morozov and Smithson (2000) showed that the amplitude decay patterns of 100- to 200-sec-long codas of these arrivals can also be consistently explained by crustal scattering. Therefore, as a cautionary, methodological outcome of this study, we note that waveform-based interpretations of mantle scattering without considering crustal effects may become biased toward increased mantle heterogeneity (for a detailed discussion of this subject, see Morozov [2001]).

Short-Period Coda of PNE Arrivals

In order to emphasize the first-order effects of reverberations within the crust and to avoid potential complications of deconvolution of relatively narrow-band, short-period (0.5–10 Hz, dominated by ~2 Hz) PNE signals complicated by scattering noise, we replace deconvolution with cross correlation of the radial (directed away from the source) and vertical components of the records. This simplification is made for three reasons. First, we did derive RF from QUARTZ records using a traditional water-level deconvolution, with the resulting interpretation of the primary reverberations close to that arising from the cross correlations presented subsequently. Second, cross-correlation does not require regularization that is typical for time- or spectral-domain deconvolution and that may become problematic for noisy short-period data. At short periods (≥1 Hz), the crustal transfer function may no longer be close to that of a stack of planar layers (e.g., Langston and Hammer, 2002) thereby invalidating the basic assumptions of RF approach. Finally, cross-correlation also represents the first step of iterative time-domain deconvolution (e.g., Ligorria and Ammon, 1999), and thus within the context of the following discussion, it can be viewed as a (limited) proxy for RFs.

The cross-correlation functions of the recordings from the three QUARTZ PNEs are trace normalized, corrected for a *Ps* travel-time delay moveout (Dueker and Sheehan, 1998) (see also equation 1 below; also note that this correction within our range of ray parameters from 0.123 to 0.09 s/km is less than 4%), and stacked at each receiver point, resulting in an image shown in Figure 3. For comparison, Figure 3 (top) also shows a detailed QUARTZ crustal and uppermost mantle velocity model derived by Morozova *et al.* (1999) by travel-time inversion of the refracted and reflected seismic phases from 51 explosions of the profile. Note that even dense coverage (10- to 15-km station spacing) was not sufficient for detailed imaging of the upper crust, and the structure of the sediments in the top and middle of Figure 3 was derived from additional, detailed DSS and industry data (Morozova *et al.*, 1999; A.V. Egorkin, 1994, personal comm.).

Comparison of the cross-correlation image with the crustal-velocity model shows good correlation of the main peak of the cross-correlation function with the depth to the basement (compare Fig. 3, middle and bottom). The pattern of cross-correlation lags is correlated with the sediment thickness, which is apparent despite the strong, apparently source reverberations that are not compensated in our simple scheme (Fig. 3, bottom). The cross-correlation peaks in our image approach zero times in the regions of the Baltic Shield, Uralian, and Altay fold belts where the sedimentary cover is thin or nearly absent and reaches 1.5–2.5 sec under the thick sedimentary covers of the Pechora and West Siberian basins. Note that the coda cross-correlation image from the PNEs allows constraining variations in the thickness of the sediments to a high degree of detail comparable to the image from detailed DSS profiling mentioned previously.

Taking advantage of the known sediment thickness along the profile QUARTZ, we can distinguish among the possible types of phases causing the observed peak in our cross correlations. The three competing hypotheses are (1) *Ps* conversion on the basement, (2) *Ppp*, or (3) *Pps* multiples within the sedimentary layers. These phases have the shortest travel-time lags after the primary *P* arrival, with the back-scattered *Pps* phase having been recently suggested to produce an important contribution to the early coda and used in RF imaging (Rondenay *et al.*, 2001).

In order to evaluate the likelihood of the three possible phase interpretations above and also to constrain the values of bulk velocities within the sediments, we consider a simple time-to-depth scaling relation for the West Siberian Basin in the middle of our profile. With time delays after the *P*-wave onset, t_D, of ~2.5 sec in and the maximum depth of the sediments, H, of ~8 km (Fig. 3), we obtain a delay per unit depth: t_D/H ~0.31 sec/km. For a *Ps*-converted mode propagating with ray parameter p, its delay after the primary *P*

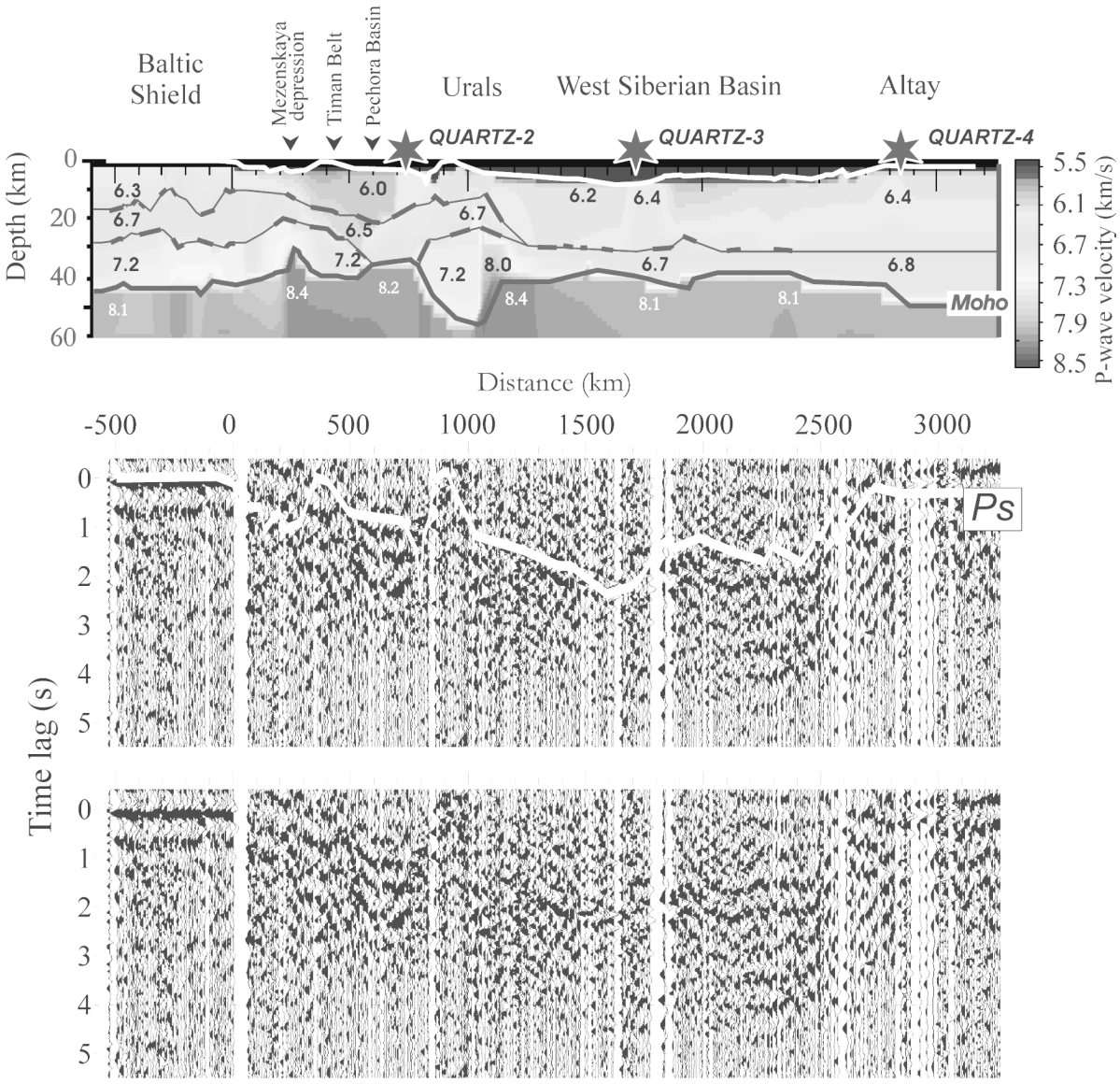

Figure 3. Mapping crustal reverberations using cross-correlated vertical and in-line components of QUARTZ records (Fig. 2). *Top*: detailed crustal and uppermost mantle velocity model from profile QUARTZ (Figure 1). The top of the basement is highlighted with a thick white line. *Bottom*: interpreted and uninterpreted stacked cross-correlation sections from the three QUARTZ PNEs, corrected for ray parameter $p = 0.09$ sec/km using equation (1). The white line in the middle plot is the profile of the basement from the crustal model (top plot) scaled to $Ps - P$ wave delay time using a factor of time/depth $= 0.31$ sec/km. Note the correspondence of the basement depth with the stacked cross correlations. Prominent reverberations at about 0.5-sec period are mostly due to the source signature.

can be related to the average velocities within the sediments, V_P and V_S (e.g., Dueker and Sheehan, 1998):

$$\frac{t_D}{H} \approx \frac{1}{V_S\sqrt{1 - (pV_S)^2}} - \frac{1}{V_P\sqrt{1 - (pV_P)^2}} - p\left(\frac{pV_S}{\sqrt{1 - (pV_S)^2}} - \frac{pV_P}{\sqrt{1 - (pV_P)^2}}\right). \quad (1)$$

In the previous expression, the first terms correspond to *S*- and *P*-wave travel times along the crustal paths, respectively, and the third term is the difference of the corresponding travel times through the mantle. Similarly, assuming that the observed cross-correlation peak is due to a *Ppp* multiple (Fig. 4, inset), we estimate its delay after the primary *P* wave as

$$\frac{t_D}{H} \approx \frac{2}{V_P\sqrt{1 - (pV_P)^2}} - p\frac{2pV_P}{\sqrt{1 - (pV_P)^2}}. \quad (2)$$

For a *Pps* phase, the corresponding travel-time lag per unit depth is

$$\frac{t_D}{H} \approx \frac{1}{V_P\sqrt{1 - (pV_P)^2}} + \frac{1}{V_S\sqrt{1 - (pV_S)^2}} - p\left(\frac{pV_P}{\sqrt{1 - (pV_P)^2}} + \frac{pV_S}{\sqrt{1 - (pV_S)^2}}\right). \quad (3)$$

We can compare the three possible interpretations above by solving equation $t_D/H = 0.31$ for V_P, with p equal to 0.09 and 0.123 sec/km and for a broad range of Poisson's ratios between $\sigma = 0.2$ and 0.45 (Fig. 4). A *Ps*-phase interpretation would fit the observations for average Poisson's ratios of $\sigma \approx 0.4$ that are significantly higher than observed in sedimentary rocks samples in lab measurements (gray shaded area in Fig. 4) (Touloukian *et al.*, 1989). An interpretation of the observed peaks as a *Ppp* multiple would also fit the observations with high but not unreasonable values of the V_P within the sediments between 5.0 and 5.5 km/sec independent on the Poisson's ratios (Fig. 4). By contrast, a *Pps* phase would produce much longer delays than *Ppp*, and therefore it would require very fast velocities $V_P > 7$ km/sec in order to fit the observed reverberation time lags (Fig. 4). Thus, based on the likelihood of required crustal velocity values, the *Pps* hypothesis is excluded, whereas both the *Ps* and *Ppp* interpretations are possible, although both are satisfied near the margins of what appears a likely sediment velocity distribution.

An additional distinction between the *Ps* and *Ppp* interpretations could potentially come from coda polarization. However, an argument based on polarization would still be inconclusive because short-period (~2 Hz) coda in a laterally heterogeneous crust (Morozova *et al.*, 1999) may exhibit complex polarization patterns inconsistent with the traditional flat-layer RF paradigm (Langston and Hammer, 2002). Thus we do not rely on polarization measurements; however, in general, observations of these phases on radial seismograms could also support the *Ps* conversion.

Our final argument in favor of the *Ps* conversion comes from comparison of the amplitudes of *Ps*-converted wave within the two end-member models of sediment velocities discussed previously and a *Ppp* multiple within a sedimentary layer of velocity 5.0 km/sec (Fig. 5). Even within the same, high-velocity sediments, the *Ps* conversion is about twice stronger in amplitude than the *Ppp* multiple, and with low sediment velocities inferred from our *Ps* interpretation of the stacked cross-correlation image, its amplitude would increase by an additional factor of ~2.5 (Fig. 5). In addition, *Ps* conversions are also more likely to be observed in radial-component recordings.

On the weight of the previous observations, we conclude that the observed coda coherence should be due primarily to a *Ps* conversion, potentially with some interference with the *Ppp* multiple. In consequence of this conclusion, the bulk Poisson's ratio of the sediments within the West Siberian basin should be between 0.35 and 0.4 (Fig. 4). Although such high values of the Poisson's ratio are not nor-

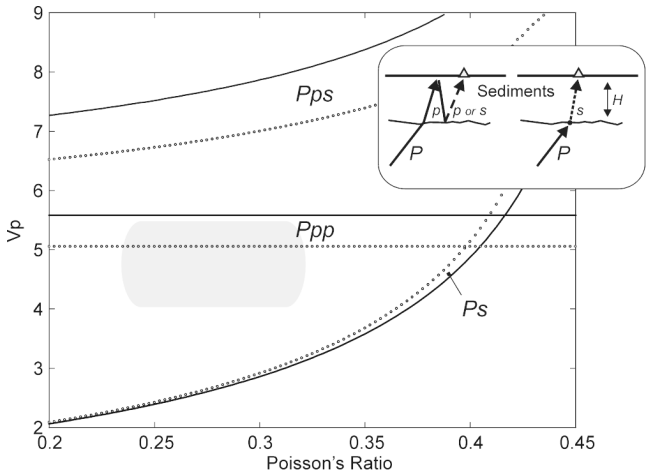

Figure 4. Regions in the *P*-wave velocity, V_P, and Poisson's ratio corresponding to $t/H = 0.31$ for a *Ps* conversion at the top of the basement and for *Ppp* or *PPs* multiples within the sedimentary layers. Solid lines correspond to ray parameter values $p = 0.09$, and dotted lines correspond to $p = 0.123$ sec/km in equations (1)–(3). Inset shows a cartoon of the phases considered; H is the thickness of the sediments. Gray shaded area indicates the region of (Vp, σ) for typical sedimentary rocks from laboratory measurements (Touloukian *et al.*, 1989).

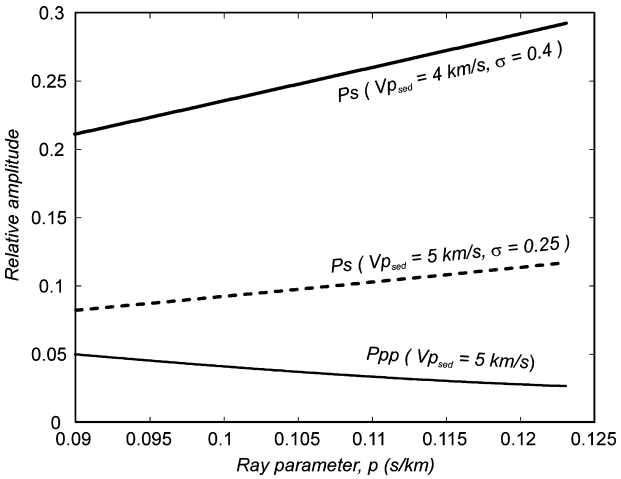

Figure 5. Amplitudes of the *Ppp* multiple and *Ps* converted phases for basement *P*-wave velocity of 6.0 km/sec and Poisson's ratio $\sigma = 0.25$ and the velocities within the sediments as labeled. Note that the *Ps* conversion is consistently higher than *Ppp* in amplitude, particularly for the sediments with high Poisson's ratio.

mally observed in laboratory measurements and appear somewhat surprising, our results suggest that they apparently could be present in large-scale sedimentary structures at seismic frequencies of ~2 Hz. At these frequencies, the *S*-wave wavelengths are about 0.8–1.5 km, and the velocities of their propagation could be affected by large-and smaller-scale fracturing, presence of fluids, scattering, and other factories leading to dispersion. These suggestions, however, are still not conclusive, and further estimates of basin-scale measurements of the Poisson's ratios at seismic frequencies are required for comparisons with our findings.

Conclusions

Coda analysis closely related to the RF technique could become both a useful imaging tool and a link between traditional travel-time and waveform inversion methods in controlled-source refraction seismology. The observed good correlation between the *Ps* or *Ppp* travel times and the depth to the basement in such a well-studied data set as QUARTZ suggests important generalizations that could be utilized in the interpretations of other long-range three-component refraction surveys: (1) peaks in cross-correlations of the vertical and radial components (and therefore in receiver functions) are due to reverberations within the sedimentary layers, (2) stacked cross-correlation or RF sections could be used to constrain variations in the depth of the basement (more precisely, travel time within the sediments) to a degree of detail that might exceed the resolution of the traditional travel-time analysis, and (3) a significant part of the observed coda is due to these strong reverberations originating within the sedimentary cover. For the part of the West Siberian Basin crossed by QUARTZ profile, our results suggest high (~0.35–0.4) average Poisson's ratios within the sediments.

In general, mode conversions and reverberations within the sedimentary column dominate the early coda of regional and teleseismic arrivals and could mask the details of the arrivals from the deeper crust and mantle. Therefore, such reverberations should be carefully considered in the interpretations of seismic scattering from within the lower crust and upper mantle.

Acknowledgments

This research was performed at the University of Wyoming reflection seismology laboratory and sponsored by the Air Force Office for Scientific Research Grants F49620-94-1-0314, F49620-94-A-0134, and the Defense Threat Reduction Agency Grant DSWA01-98-0015. Seismic data from the PNE profile QUARTZ were provided by the Center GEON, Moscow, as a part of its cooperation with University of Wyoming in the archiving and analysis of the DSS data.

References

Ammon, C. J. (1991). The isolation of receiver effects from teleseismic *P* waveforms, *Bull. Seism. Soc. Am.* **81,** 2504–2510.

Ammon, C. J., G. E. Randall, and G. Zandt (1990). On the nonuniqueness of receiver function inversions, *J. Geophys. Res.* **95,** 15,303–15,318.

Bostock, M. G. (1996). Ps conversions from the upper mantle transition zone beneath the Canadian landmass, *J. Geophys. Res.* **101,** 8393–8402.

Chevrot, S., L. Vinnik, and J. P. Montagner (1999). Global-scale analysis of the mantle *Pds* phases, *J. Geophys. Res.* **104,** 20,203–20,219.

Dueker, K. G., and A. F. Sheehan (1998). Mantle discontinuity structure beneath the Colorado Rocky Mountains and High Plains, *J. Geophys. Res.* **103,** 7153–7169.

Egorkin, A. V., and A. V. Mikhaltsev (1990). The results of seismic investigations along geotraverses, in *Super-Deep Continental Drilling and Deep Geophysical Sounding*, K. Fuchs, Y. A. Kozlovsky, A. I. Krivtsov, and M. D. Zoback (Editors), Springer, Berlin, 111–119.

Gurrola, H., and J. B. Minster (2000). Evidence for local variations in the depth to the 410-km discontinuity beneath Albuquerque, New Mexico, *J. Geophys. Res.* **105,** 10,847–10,856.

Henstock, T. J., A. R. Levander, C. M. Snelson, G. R. Keller, K. C. Miller, S. H. Harder, A. R. Gorman, R. M. Clowes, M. J. A. Burianyk, E. D. Humphreys, (1998). Probing the Archean and Proterozoic lithosphere of western North America, *GSA Today* **8,** 1–5.

Langston, C. A. (1977). The effect of planar dipping structure on source and receiver responses for constant ray parameter, *Bull. Seism. Soc. Am.* **67,** 1029–1050.

Langston, C. A., and J. K. Hammer (2002). The vertical component P-wave receiver function, *Bull. Seism. Soc. Am.* **91,** 1805–1819.

Ligorria, J. P., and C. J. Ammon (1999). Iterative deconvolution and receiver-function estimation, *Bull. Seism. Soc. Am.* **89,** 1395–1400.

Mechie, J., A. V. Egorkin, K. Fuchs, T. Ryberg, L. Solodilov, and F. Wenzel (1993). P-wave velocity structure beneath northern Eurasia from long-range recordings along the profile QUARTZ, *Phys. Earth Planet, Interiors* **79,** 269–286.

Morozov, I. B. (2001). Comment on "High-frequency wave propagation in the uppermost mantle" by T. Ryberg and F. Wenzel, *J. Geophys. Res.* **106,** 30,715–30,718.

Morozov, I. B., E. A. Morozova, and S. B. Smithson (1998a). On the nature of the teleseismic *Pn* phase observed in the recordings from the ultra-long profile "Quartz", Russia, *Bull. Seism. Soc. Am.* **88,** 62–73.

Morozov, I. B., E. A. Morozova, S. B. Smithson, and L. N. Solodilov, (1998b). 2-D image of seismic attenuation beneath the Deep Seismic Sounding profile QUARTZ, Russia, *Pure Appl. Geophys.* **153,** 311–343.

Morozov, I. B., and S. B. Smithson (2000). Coda of long-range arrivals from nuclear explosions, *Bull. Seism. Soc. Am.* **90,** 929–939.

Morozova, E. A., I. B. Morozov, S. B. Smithson, and L. N. Solodilov (1999). Heterogeneity of the uppermost mantle beneath the ultra-long range profile "Quartz," Russian Eurasia, *J. Geophys. Res.* **104,** 20,329–20,348.

Morozova, E. A., I. B. Morozov, S. B. Smithson, and L. N. Solodilov (2000). Lithospheric boundaries and upper mantle heterogeneity beneath Russian Eurasia: evidence from the DSS profile QUARTZ, *Tectonophysics* **329,** 333–344.

Rondenay, S., M. G. Bostock, and J. Shragge, J. (2001). Multiparameter two-dimensional inversion of scattered teleseismic body waves. III. Application to the Cascadia 1993 data set, *J. Geophys. Res.* **106,** 30,795–30,807.

Ryaboy, V. (1989). *Upper Mantle Structure Studies by Explosion Seismology in the USSR*, Delphic Associates, Falls Church, Virginia, 138 pp.

Ryberg, T., K. Fuchs, A. V. Egorkin, and L. Solodilov (1995). Observations of high-frequency teleseismic *Pn* on the long-range Quartz profile across northern Eurasia, *J. Geophys. Res.* **100,** 18,151–18,163.

Ryberg, T., M. Tittgemeyer, and F. Wenzel (2000). Finite difference modeling of P-wave scattering in the upper mantle, *Geophys. J. Int.* **141,** 787–800.

Ryberg, T., F. Wenzel, J. Mechie, A. Egorkin, K. Fuchs, and L. Solodilov (1996). Two-dimensional velocity structure beneath Northern Eurasia

derived from the super long-range seismic profile Quartz, *Bull. Seism. Soc. Am.* **86,** 857–867.

Schueller, W., I. B. Morozov, and S. B. Smithson (1997). Crustal and uppermost mantle velocity structure of northern Eurasia along the profile Quartz, *Bull. Seism. Soc. Am.* **87,** 414–426.

Thybo, H., and E. Perchuc (1997). The seismic 8° discontinuity and partial melting in continental mantle, *Science* **275,** 1626–1629.

Tittgemeyer, M., F. Wenzel, K. Fuchs, and T. Ryberg (1996). Wave propagation in a multiple-scattering upper mantle—observations and modeling, *Geophys. J. Int.* **127,** 492–502.

Touloukian, Y. S., W. R. Judd, and R. F. Roy (Editors) (1989). Physical properties of rocks and minerals, in *CINDAS Data Series on Material Properties, Group II: Properties of Special Materials*, Hemisphere Publishing Co., New York, Vol. II-2, 221–256.

Vinnik, L. P. (1977). Detection of waves converted from *P*-to-*SV* in the mantle, *Phys. Earth Planet Interiors* **15,** 294–303.

Yegorkin, A. V. (1992). Crustal structure along seismic geotraverses, *Int. Geol. Rev.* **34,** 345–362.

Department of Geology and Geophysics
University of Wyoming
PO Box 3006, Laramie, Wyoming 82071-3006
(I.B.M., S.B.S.)

Centre for Regional Geophysical and Geoecological Research (GEON)
Moscow, Russia
(L.N.S.)

Manuscript received 24 January 2002.